Journal of chemical & engineering data

Article

Cite This: J. Chem. Eng. Data 2019, 64, 4724−4732

pubs.acs.org/jced

Adsorption Equilibrium of Carbon Dioxide, Methane, Nitrogen, Carbon Monoxide, and Hydrogen on UiO-66(Zr)_(COOH)$_2$

M. A. Moreira,[†] R. O. M. Dias,[†] U.-Hwang Lee,[‡] Jong-San Chang,*[,‡,§] A. M. Ribeiro,[†] A. F. P. Ferreira,[†] and A. E. Rodrigues*[,†]

[†]Laboratory of Separation and Reaction Engineering, Associate Laboratory LSRE/LCM, Department of Chemical Engineering, Faculty of Engineering, University of Porto, Rua Dr. Roberto Frias s/n, 4200-465 Porto, Portugal

[‡]Catalysis Center for Nanocatalysts, Korea Research Institute of Chemical Technology (KRICT), Jang-dong 100, Yuseong, Daejeon, Korea

[§]Department of Chemistry, Sungkyunkwan University, Suwon 440-476, Korea

S *Supporting Information*

ABSTRACT: Process intensification, with the aim of reducing the energy consumption of the existing processes, opens the path to exploring diverse operating conditions. As far as adsorption-based processes are concerned, cryogenic temperatures and high pressures are less-explored conditions. In this work, the adsorption equilibria of carbon dioxide, methane, carbon monoxide, nitrogen, and hydrogen are assessed at temperatures of between 223 and 373 K and at pressures of up to 60 bar for acid-functionalized UiO-66(Zr) MOF, the UiO-66(Zr)_(COOH)$_2$, shaped as small granules. UiO-66(Zr)_(COOH)$_2$ is selective for carbon dioxide, presenting the highest adsorption capacities among all of the tested gases. The adsorption capacity then follows the order methane, nitrogen, carbon monoxide, and hydrogen. Indeed, the very low capacity toward carbon monoxide is a remarkable feature of this material. The carbon dioxide/methane ideal selectivity at 220 K, 40 bar, and a feed composition of 99% methane and 1% carbon dioxide is 44. The isosteric heats of adsorption mirror the adsorption capacity, carbon dioxide has an adsorption heat of between 40 and 20 kJ·mol^{-1}, and methane has a adsorption heat of between 25 and 10 kJ·mol^{-1}. Nitrogen and carbon monoxide have the lowest adsorption heats of about 20−10 and 15−10 kJ·mol^{-1}, respectively. Thus, UiO-66(Zr)_(COOH)$_2$ presents a high potential for relevant industrial processes such as the natural gas/biogas upgrade, hydrogen production, and syngas composition tuning.

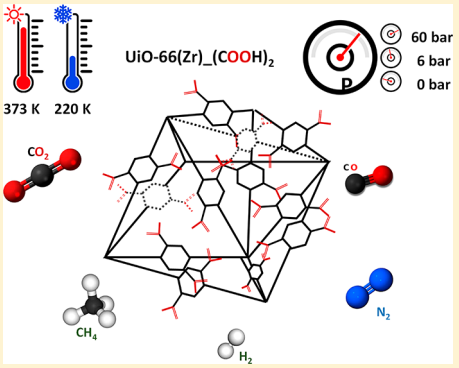

INTRODUCTION

To efficiently use adsorption-based processes in industrial applications, it is vital to fully comprehend the adsorption properties of a material regarding some important gases from an industrial standpoint. Although extensive work on gas adsorption in various porous solids at ambient temperatures or above is available, there is a lack of data existing in the open literature for extreme conditions (i.e., cryogenic temperatures and high pressures). Hydrogen storage[1−3] and natural gas purification[2,4,5] are some industrial applications where cryo-adsorptive methods are being reviewed.

Hydrogen has been studied as a clean energy source for transportation because of its high energy density and carbon-free combustion products. Various studies have been done on hydrogen storage in MOFs for further implementation in fuel cell technologies because hydrogen is particularly hard to liquefy or compress given its low boiling point (20 K).[2,3] With the use of metal−organic frameworks (MOFs), it is possible to retain hydrogen at 77 K and at a pressure of less than 100 bar, which requires much less energy than traditional cryogenic hydrogen tanks.[2] However, as the temperature increases, the H_2 uptake dramatically decreases, with a gravimetric capacity that does not exceed 0.5 wt % at ambient temperature.[1] According to the U.S. Department of Energy, the 2025 H_2 storage targets are 5.5 wt % in gravimetric capacity and 40 g·L^{-1} in volumetric capacity at an operating temperature of 233 to 353 K under a maximum delivery pressure of 12 bar.[6] None of the materials studied so far have met the DOE standards.

Natural gas (NG) has also been considered to be an alternative for petroleum-based fuels because CH_4 has the highest H to C ratio of any fossil fuel, and for this reason, the combustion of this gas results in less CO and CO_2 released per unit of energy generated.[7] Despite this, one of the main challenges presented is the energy density of natural gas at ambient temperature and pressure, which is only 0.04 MJ·L^{-1}, compared to 32.4 MJ·L^{-1} for gasoline.[7] To overcome this, NG can be liquefied, reaching a volumetric energy density of 20.8

Special Issue: Celebrating Our High Impact Authors

Received: January 15, 2019
Accepted: March 29, 2019
Published: April 10, 2019

DOI: 10.1021/acs.jced.9b00053
J. Chem. Eng. Data 2019, 64, 4724−4732

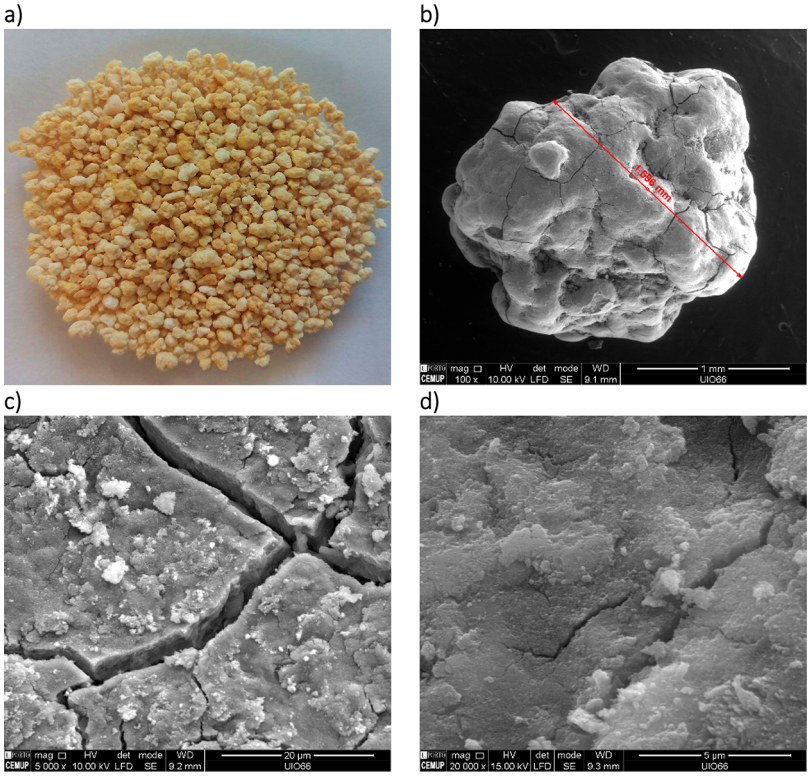

Figure 1. UiO-66(Zr)_$(COOH)_2$ agglomerates: (a) as supplied by KRICT; (b) SEM image of a granulate magnified 100×; (c) SEM image of the crystals in a granule's surface magnified 5000×; and (d) SEM image of the crystals in a granule's interior magnified 20 000×.

$MJ{\cdot}L^{-1}$. One of the major pollutants in liquified natural gas (LNG) is CO_2, which can solidify and block pipelines, generating transportation drawbacks.[5] For this matter, purification of the gas stream is needed. Although this can be done by various methods, the adsorption-based CO_2 separation is appealing because of its lower energy requirements. MOFs are promising materials for CO_2 separation because of the interaction between molecules and the framework and the resulting selective adsorption of the gas. When the final product is LNG, cryogenic separation is of particular interest. Hydrogen purification ($H_2/(CO + CO_2)$), syngas composition tuning ($(H_2 + CO)/CO_2$), and CO_2 capture from flue gas (CO_2/N_2)[2,8] are industrial processes for which cryogenic adsorption processes have not yet been reviewed. Nevertheless, the study of the adsorption equilibrium of these adsorbates at low temperatures might be useful for future prospects.

In this work, we study the adsorption properties of a type of Zr-MOF that, according to Yang et al.,[9] has optimal features for CO_2 capture: UiO-66-BTEC. UiO-66-BTEC, also referred to in the literature as UiO-66-$(COOH)_2$,[9,10] is built up from zirconium oxide clusters, $[Zr_6O_4(OH)_4]$, connected to 1,2,4,5-benzenetetracarboxylate (BTEC) linkers instead of the non-functionalized UiO-66, which is linked to 1,4-benzenedicarboxylate (BDC), giving it two carboxylic acid functional groups. This leads to an overall porous cubic structure, showing a central octahedral cage surrounded by tetrahedral cages, linked by constricted triangular windows.[11,12] In contrast to other MOFs, which, compared to traditional adsorbents such as zeolites, lack thermal, hydrothermal, and chemical stability, UiO-66-type MOFs were shown to be thermally stable (up to 813 K) and to have prominent water stability.[13,14] Although the pristine form has a Langmuir surface area of 1187 $m^2{\cdot}g^{-1}$ and a pore volume of 0.45 $cm^3{\cdot}g^{-1}$,[13] it is known that the presence of moieties in the linker tends to reduce this value as well as the pore volume. According to Yang et al., the theoretically accessible surface area is 428 $m^2{\cdot}g^{-1}$ and the pore volume is 0.26 $cm^3{\cdot}g^{-1}$.[9,11] However, they can be used to increase the interaction of the framework with various adsorbates.[15] In this particular case, the two acidic functions strongly interact with CO_2 molecules, allowing the selective capture of CO_2 from different mixtures.[9,11]

Regarding the performance of UiO-66-BTEC, not many adsorption equilibrium data can be found in the literature. Yang et al.[9] obtained the N_2 isotherm at 77 K, and Ragon et al.[11] reported equilibrium isotherms for CO_2 and CH_4 at 303 K over a pressure range of 0−25 bar. Relating to low-temperature adsorption, Cavenati et al.[4] published an article on the cryogenic adsorption of CO_2 and CH_4 in zeolites 4A and 13X, and more recently, Moreira et al.[5] also obtained equilibrium data for the same compounds, with temperatures ranging from 180 to 473 K and pressures reaching 80 bar. Information related to low-temperature adsorption in the target material is not available in the open literature.

This said, the scope of this work is to assess the adsorption properties of the UiO-66-BTEC metal−organic framework with respect to the gases involved in the aforementioned industrial processes over broad temperature and pressure ranges. Therefore, adsorption equilibrium isotherms of pure H_2, N_2, CO, CO_2, and CH_4 in shaped UiO-66-BTEC MOF are reported here. These isotherms were measured at temperatures of between 223 and 373 K and at pressures of up to 60 bar.

EXPERIMENTAL SECTION

Adsorbent Material and Reagents. The adsorbent tested in this work was UiO-66(Zr)_$(COOH)_2$, synthesized

DOI: 10.1021/acs.jced.9b00053
J. Chem. Eng. Data 2019, 64, 4724−4732

and shaped in the form of agglomerates at the Korea Research Institute of Chemical Technology (KRICT).

The UiO-66(Zr)_$(COOH)_2$ agglomerates were morphologically characterized by scanning electron microscopy (SEM) and energy-dispersive X-ray spectroscopy (EDS). The SEM and EDS analyses were performed using a high-resolution environmental scanning electron microscope (Schottky) with X-ray microanalysis and electron backscattered diffraction analysis (Quanta 400 FEG ESEM/EDAX Genesis X4M). N_2 adsorption/desorption at 77 K was determined with an ASAP 2420 V2.09 (V2.09 J). The t-plot method was used to estimate the micropore volume, and the surface area was determined by the Brunauer, Emmett, and Teller (BET) method. N_2 adsorption analysis was performed after degassing the sample at 423 K for 3 h under vacuum. The skeleton density of the granules was determined by helium pycnometry, and the apparent density was determined by mercury (Hg) intrusion at low pressures (3 bar). Hg porosimetry analysis was performed on the granules, as provided, using a Micromeritics AutoPore IV 9500 (V1.07).

Carbon dioxide, methane, carbon monoxide, nitrogen, hydrogen, and helium were supplied by Air Liquide, with purities greater than 99.99%.

Multigram-Scale Powder Synthesis. In a round-bottomed flask equipped with a reflux condenser and magnetic stirrer, 43 g (0.17 mol) of 1,2,4,5-benzenetetracarboxylic acid (BTEC) (Aldrich, >97%) and 23 g (0.10 mol) of zirconium tetrachloride ($ZrCl_4$) (Aldrich, 98%) were dissolved in 500 mL of distilled water (27.8 mol) at room temperature under stirring and then heated under reflux (~100 °C) for 24 h. The resulting white gel was filtered off and washed with water at room temperature. The solid was dispersed in distilled water (~10 mL per 1 g of product) and held under reflux for 16 h. The solid was then recovered by filtration, thoroughly washed with acetone, and dried at 30 °C under vacuum, yielding ~40 g of white powder.

Large-Scale Powder Synthesis. For the synthesis of functionalized UiO-66(Zr)_$(COOH)_2$, zirconium tetrachloride and 1,2,4,5-benzenetetracarboxylic acid were soaked in a glass reactor (20 L scale) containing distilled water. Accompanied by mechanical stirring of the solutions, the reactor temperature was increased up to 100 °C. After purification, the obtained MOF was dried at 100 °C for 12 h.

Granulate Shaping. MOF shaping in the form of spherical granulates was performed using a granulation method. In the first step, the powder was mixed with 3−10 wt % of an organic binder. The mixture of the MOF powder and binder was shaped by a homemade granulator. Before granulation, powder samples were finely ground with a ball mill machine with zirconia balls in order to obtain a fine similar particle size. Then, water and ethanol were periodically sprayed on the solid mixture to allow the agglomeration of the powder. As a result of granulation, semispherical-type particles with a size range of between 1.0 and 3.0 mm were formed (Figure 1).

Equipment and Procedure. The adsorption equilibrium measurements of pure components were performed using a gravimetric method (Rubotherm magnetic suspension balance), with a precision of 10 μg and operated in a closed system. The system comprises a basket where the adsorbent is placed, which is linked to a permanent magnet placed in the adsorption chamber. This permanent magnet works together with an electromagnet that is connected to an analytical balance, making it possible to measure the weight variations of the system. The major advantage of this equipment is the possibility to operate in a wide temperature range because it can be used with a cold gas cooling jacket or an electrical heater. More information about this equipment can be found somewhere else.[5]

Adsorption equilibrium isotherms were determined at 223, 273, 303, 333, and 373 K up to 60 bar. According to the desired temperatures, the system was cooled or heated, and pure feed gas was introduced into the magnetic suspension balance, step by step, waiting for equilibrium to be achieved in between steps. Over time, all adsorbent weight differences, pressure increments, and temperature inside the adsorption chamber were recorded by a computer. Prior to adsorption experiments, the adsorbent sample was weighed and placed in a basket to be activated. Sample activation was performed under vacuum at 423 K overnight, resulting in a sample mass loss of 11.8%. The equilibrium was considered to be achieved when the change in weight was less than 0.1 mg in 30 min. However, if equilibrium was achieved in less than 120 min, then the minimum waiting time would be 120 min.

In the adsorption capacity calculation, the buoyancy effect was taken into consideration and corrected, assuming that the density of the adsorbed phase is equal to the density of the liquid (eq 1).

$$q = \frac{\Delta m + (V_s + V_c) \times \rho_g}{m_s M} \frac{\rho_l}{\rho_l - \rho_g} \tag{1}$$

Δm represents the mass difference between the mass given by the microbalance and the initial mass of the basket loaded with the activated sample. V_s is the volume of the solid adsorbent, V_c is the volume of inert parts, and ρ_g is the density of the gas under measurement conditions. The adsorbed phase density (ρ_l) can be calculated from the molar mass (M) and the molar volume (υ), as presented in eq 2.

$$\rho_l = \frac{M}{\upsilon} \tag{2}$$

The molar volume (υ) can be estimated from several semiempirical methods, some of them temperature-dependent.[16] In this work, it was assumed that below the critical temperature, the molar volume can be determined by eq 3.

$$\upsilon = \upsilon_b + \frac{T - T_b}{T_c - T_b}(b - \upsilon_b) \tag{3}$$

T_c and T_b (K) are the critical and boiling-point temperatures, respectively, and υ_b ($cm^3\ mol^{-1}$) and b ($cm^3\ mol^{-1}$) are the molar volume at T_b and the van der Waal's volume, respectively. However, above the critical temperature, υ is assumed to be equal to the van der Waal's volume (eq 4).[16,17] More details about the buoyancy effect correction methodology and molar volume estimation can be found elsewhere.[5,16−18]

$$\upsilon = b \tag{4}$$

RESULTS AND DISCUSSION

UiO-66(Zr)_$(COOH)_2$ Characterization. UiO-66(Zr)_$(COOH)_2$ granules were characterized by SEM and EDS analysis. SEM images shown in Figure 1 reveal that the material consists of homogeneous agglomerates of around 1.6 mm. According to EDS analysis (Figure 2), it detected zirconium, carbon, and oxygen in large quantities, which is

DOI: 10.1021/acs.jced.9b00053
J. Chem. Eng. Data 2019, 64, 4724−4732

consistent with inorganic oxocluster $Zr_6O_4(OH)_4$ and the organic linker used during the synthesis.

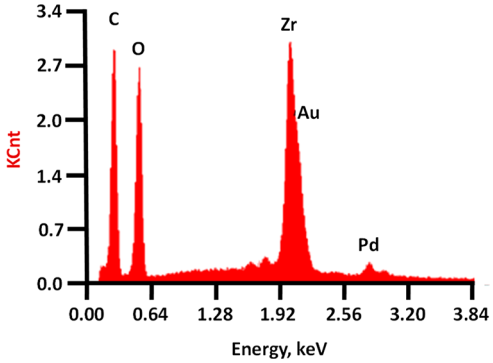

Figure 2. UiO-66(Zr)_$(COOH)_2$EDS analysis.

The adsorbent was characterized by the adsorption of N_2 at 77 K. The values obtained for the micropores volume (V_{micro}), total pore volume (V_{total}), and surface areas are summarized in Table 1. The assessed adsorption equilibrium isotherms of N_2

Table 1. Textural Properties of the UiO-66(Zr)_$(COOH)_2$ Agglomerates

properties	UiO 66(Zr)_$(COOH)_2$	units
$S_{Langmuir\ surface\ area}$	568	$m^2 \cdot g^{-1}$
$S_{t\text{-}plot\ micropore\ area}$	451	$m^2 \cdot g^{-1}$
V_{macro}	0.727	$cm^3 \cdot g^{-1}$
V_{micro}	0.142	$cm^3 \cdot g^{-1}$
ρ_{sk}	1.82	$g \cdot cm^{-3}$
$\rho_{s,Hg}$	1.63	$g \cdot cm^{-3}$
ρ_{ap}	0.75	$g \cdot cm^{-3}$
d_p	0.03	μm

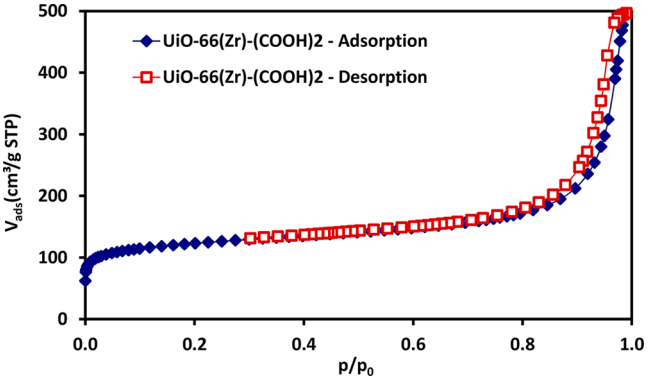

Figure 3. N_2 adsorption equilibrium isotherms on UiO-66(Zr)_$(COOH)_2$ agglomerates at 77 K. Closed and open symbols correspond to the adsorption and desorption branches, respectively.

at 77 K are also reported in Figure 3. Apparent (ρ_{ap} = mass of solid/granule volume), solid ($\rho_{s,Hg}$ = mass of solid/(granule volume − (macro + meso) pore volume)), and skeleton (ρ_{sk} = mass of solid/(granule volume − (macro + meso + micro) pore volume)) densities of the granules, obtained by mercury intrusion and helium pycnometry, are also reported in Table 1. In Figure 4, the macropore/mesopore size distribution obtained by mercury intrusion is presented. It can be observed

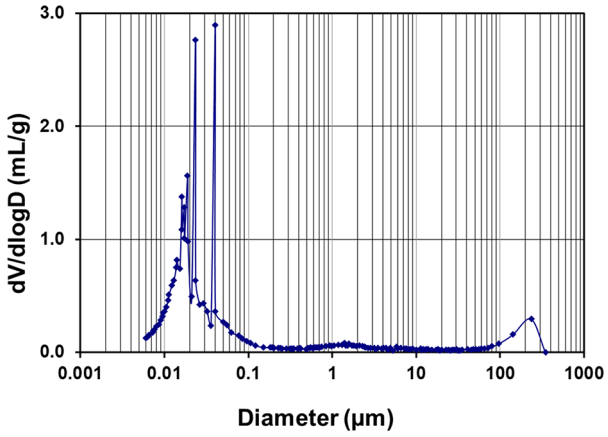

Figure 4. Intercrystalline macropore size distribution by mercury intrusion of UiO-66(Zr)_$(COOH)_2$ agglomerates.

that the median macropore diameter (volume base), derived from the shaping (secondary pore network), is 0.03 μm, as reported in Table 1. For comparison, information on the powder characterization can be found in the Supporting Information (SI).

Adsorption Equilibrium Measurements. The adsorption equilibrium isotherms were determined for carbon dioxide, methane, carbon monoxide, nitrogen, and hydrogen on UiO-66(Zr)_$(COOH)_2$ at the temperatures and maximum pressures presented in Table 2.

Table 2. Summary of the Adsorption Equilibrium Measurements Performed on UiO-66(Zr)_$(COOH)_2$

	P_{max} (bar)				
T (K)	CO_2	CH_4	N_2	CO	H_2
373	60	60	60		
333	60	60	60	5	30
303	60	60	60	5	30
273	30	60	60	5	30
223	6	60	60		

The results obtained are shown as points in Figure 5. The closed symbols represent points measured as the pressure was being increased, and the open ones were measured by decreasing the adsorption cell's pressure. It is possible to observe that the closed symbols are aligned with the open symbols, making it possible to conclude that the isotherms are reversible because no hysteresis is observed. It is also possible to note that the adsorbent presents a higher adsorption capacity for carbon dioxide, followed by methane, carbon monoxide, nitrogen, and hydrogen. The absolute amounts adsorbed for each gas, at different temperatures, are shown in Tables 3, 4, 5, 6, and 7.

Adsorption equilibrium isotherms of carbon dioxide and methane reported in this work at 303 K and up to 25 bar are compared to the data reported by Ragon et al.[11] in Figure 6. One must call to readers' attention the fact that data reported by Ragon and co-workers was obtained in a powder sample and synthesized on a small scale, whereas the sample used in this work was shaped into granules and the original powder was synthesized on the killigram scale. Even then, the results are in very good agreement, which can indicate the high quality of the shaped sample, with very low capacity reduction due to

DOI: 10.1021/acs.jced.9b00053
J. Chem. Eng. Data 2019, 64, 4724−4732

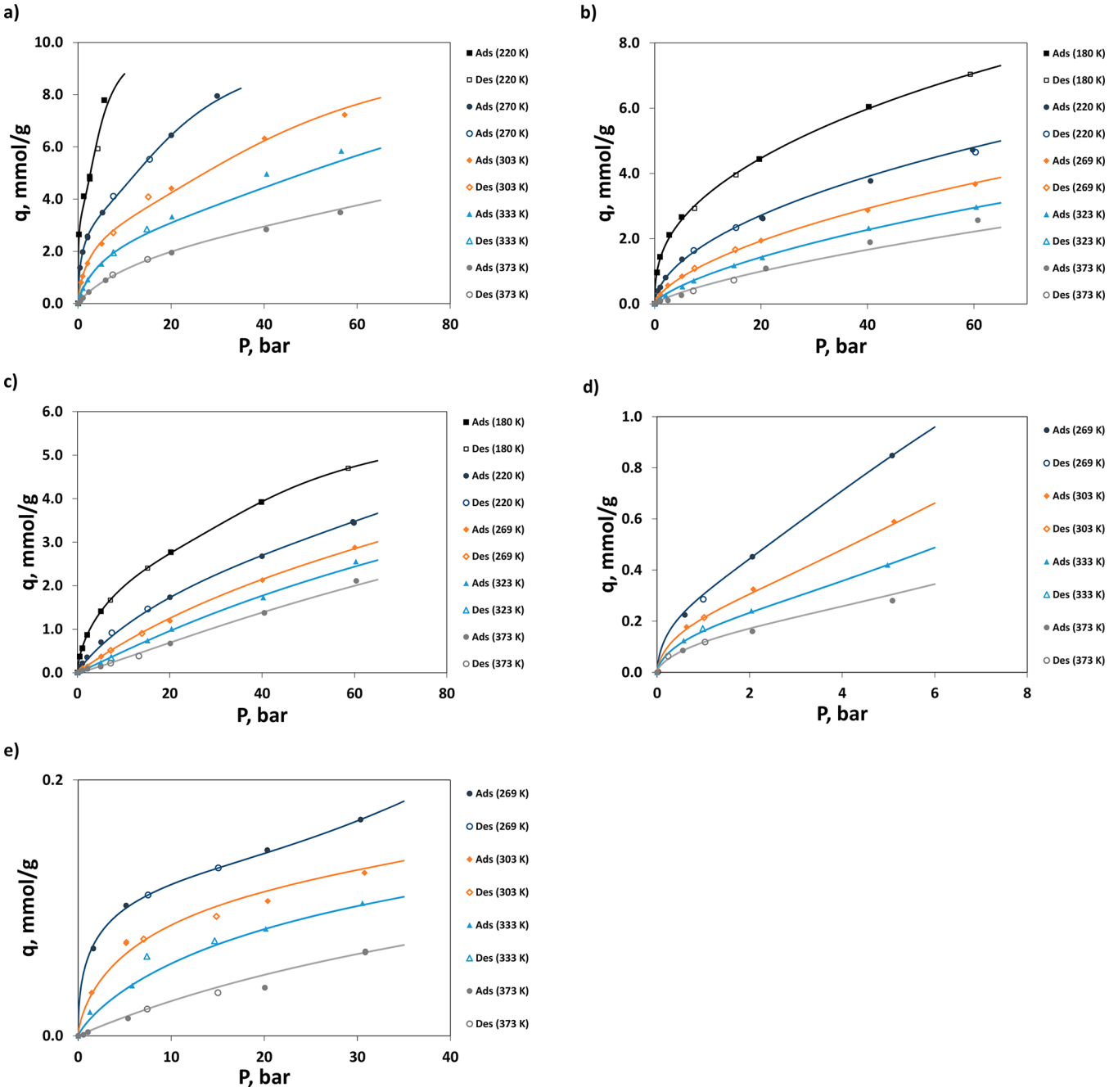

Figure 5. Adsorption equilibrium isotherms on UiO-66(Zr)_$(COOH)_2$ for (a) carbon dioxide, (b) methane, (c) nitrogen, (d) carbon monoxide, and (e) hydrogen at 223, 273, 303, 333, and 373 K. Symbols represent the experimental data, and solid lines represent the dual-site Sips isotherm fit.

shaping. In fact, the granulation protocol previously described retains the high porosity of the material and leads to a loss of surface area of less than 18%.

Figure 7 compares the adsorption equilibrium of carbon dioxide and methane on UiO-66(Zr)_$(COOH)_2$ granules and on binderless zeolite 13X beads reported by Moreira et al.[5] This comparison highlights the potential of UiO-66(Zr)_$(COOH)_2$ MOF for cryo-PTSA applications (i.e., the regeneration of the bed by increasing the temperature and decreasing the pressure will be more efficient for UiO-66(Zr)_$(COOH)_2$, allowing higher CO_2 working capacities for the same operating conditions reported by Moreira et al.[5]). However, the ideal selectivity at 220 K, 40 bar, and a feed composition of 99% methane and 1% carbon dioxide, similar to the feed conditions reported by Moreira and co-workers[5] for the cryo-PTSA process, is 44 for UiO-66(Zr)_$(COOH)_2$, whereas for binderless zeolite 13X, it was about 124. The potential of UiO-66(Zr)_$(COOH)_2$ for a natural gas upgrade is due to the combination of chemical and thermal stability with a moderate isosteric heat of adsorption toward CO_2, allowing adsorbent regeneration with low energy consumption (vacuum or temperature).

The low adsorption capacity toward CO when compared to CO_2 is a peculiar characteristic of this material. In Figure 8, the adsorption capacity of carbon monoxide on UiO_66(Zr)_BTEC is compared with that of other materials such as

DOI: 10.1021/acs.jced.9b00053
J. Chem. Eng. Data 2019, 64, 4724−4732

Table 3. Experimental Data of Carbon Dioxide Adsorption Equilibrium on UiO-66(Zr)_$(COOH)_2$ at 220, 270, 303, 333, and 373 K

T = 220 K		T = 270 K		T = 303 K		T = 333 K		T = 373 K	
P	q	P	q	P	q	P	q	P	q
(bar)	(mmol·g^{-1})	(bar)	(mmol·g^{-1})	(bar)	(mmol·g^{-1})	(bar)	(mmol·g^{-1})	(bar)	(mmol·g^{-1})
0.01	0.00	0.01	0.00	0.01	0.00	0.00	0.00	0.00	0.00
0.19	2.65	0.42	1.37	0.66	0.81	0.58	0.36	0.54	0.11
1.23	4.11	0.99	1.97	0.99	1.05	0.58	0.36	1.04	0.21
2.50	4.86	2.05	2.57	2.04	1.54	1.09	0.59	2.31	0.44
2.52	4.78	2.07	2.53	5.06	2.29	2.08	0.92	5.93	0.89
5.64	7.79	5.26	3.48	5.06	2.30	5.06	1.52	20.12	1.95
4.26	5.93	20.03	6.44	20.07	4.41	20.19	3.32	40.46	2.84
		29.90	7.95	40.07	6.32	40.55	4.97	56.37	3.49
		15.39	5.52	57.33	7.23	56.60	5.84	14.96	1.69
		7.60	4.11	15.09	4.09	14.82	2.85	7.48	1.10
				7.56	2.72	7.60	1.94		

Table 4. Experimental Data of Methane Adsorption Equilibrium on UiO-66(Zr)_$(COOH)_2$ at 219, 269, 303, 333, and 373 K

T = 219 K		T = 269 K		T = 303 K		T = 333 K		T = 373 K	
P	q	P	q	P	q	P	q	P	q
(bar)	(mmol·g^{-1})	(bar)	(mmol·g^{-1})	(bar)	(mmol·g^{-1})	(bar)	(mmol·g^{-1})	(bar)	(mmol·g^{-1})
0.01	0.00	0.00	0.00	0.02	0.00	0.00	0.00	0.00	0.00
0.41	0.97	0.62	0.40	0.59	0.17	0.72	0.11	0.53	0.05
0.43	0.96	1.06	0.51	1.07	0.29	1.09	0.17	1.07	0.09
1.01	1.44	2.05	0.80	2.48	0.57	2.09	0.26	2.49	0.11
2.73	2.11	5.14	1.36	5.15	0.84	5.22	0.53	5.03	0.27
5.05	2.66	20.12	2.65	5.15	0.85	20.24	1.42	20.91	1.08
19.66	4.44	20.32	2.62	19.99	1.94	40.21	2.32	20.91	1.09
40.23	6.04	40.58	3.77	40.05	2.87	60.44	2.97	40.49	1.89
59.33	7.04	59.77	4.72	60.24	3.67	14.93	1.18	60.74	2.57
15.29	3.95	60.30	4.65	15.16	1.67	7.34	0.71	14.88	0.73
7.49	2.93	15.29	2.34	7.53	1.09			7.27	0.40
		7.36	1.64						

Table 5. Experimental Data of Nitrogen Adsorption Equilibrium on UiO-66(Zr)_$(COOH)_2$ at 219, 269, 303, 333, and 373 K

T = 219 K		T = 269 K		T = 303 K		T = 333 K		T = 373 K	
P	q	P	q	P	q	P	q	P	q
(bar)	(mmol·g^{-1})	(bar)	(mmol·g^{-1})	(bar)	(mmol·g^{-1})	(bar)	(mmol·g^{-1})	(bar)	(mmol·g^{-1})
0.03	0.00	0.03	0.00	0.02	0.00	0.00	0.00	0.03	0.00
0.49	0.37	0.59	0.14	0.63	0.06	0.64	0.04	0.61	0.03
1.07	0.56	1.08	0.22	1.12	0.10	1.19	0.07	1.09	0.05
1.07	0.56	2.08	0.36	2.18	0.15	2.05	0.12	2.19	0.08
2.10	0.87	5.10	0.70	5.13	0.37	5.05	0.24	5.05	0.14
5.09	1.41	20.05	1.73	5.13	0.37	20.39	1.01	5.03	0.14
20.22	2.77	39.99	2.68	20.02	1.19	20.38	1.01	20.12	0.67
39.83	3.92	59.68	3.47	40.06	2.13	40.25	1.73	40.47	1.38
58.64	4.70	59.88	3.44	60.10	2.88	60.30	2.56	60.38	2.11
15.21	2.40	15.24	1.46	13.97	0.90	15.20	0.74	13.33	0.38
7.15	1.67	7.46	0.92	7.22	0.51	7.31	0.35	7.20	0.22

MOFs,[19] activated carbons,[20] and zeolites[20,21] at 303 K. The CO_2/CO ideal selectivity for this material is 4.2 at 303 K and 4 bar with a feed composition of 30% CO_2, 22% CO, and 48% H_2.[19] This characteristic can be exploited for syngas composition tuning (CO_2/CO separation). The selectivity of this material is comparable to that of the other reported materials: 9.2, MIL-125(Ti)_NH_2;[19] 4.3, activated carbon;[20] and 3.1, zeolite.[20]

Adsorption equilibrium isotherms are one of the principal pieces of information required while designing an adsorption process. There are several adsorption equilibrium models that can be used to represent the experimental adsorption equilibrium results. In this study, the dual-site Sips (DSS) model was used because it is the one that best represented the experimental data (eq 5). The dual-site nature of the UiO-66(Zr)_BTEC material (i.e., its structure is composed of tetrahedral cages and larger octahedral cages) is a reasonable

DOI: 10.1021/acs.jced.9b00053
J. Chem. Eng. Data 2019, 64, 4724−4732

Table 6. Experimental Data of Carbon Monoxide Adsorption Equilibrium on UiO-66(Zr)_$(COOH)_2$ at 269, 303, 333, and 373 K

T = 269 K		T = 303 K		T = 333 K		T = 373 K	
P	q	P	q	P	q	P	q
(bar)	(mmol·g^{-1})	(bar)	(mmol·g^{-1})	(bar)	(mmol·g^{-1})	(bar)	(mmol·g^{-1})
0.03	0.00	0.01	0.00	0.00	0.00	0.00	0.00
0.60	0.22	0.64	0.18	0.58	0.12	0.56	0.09
2.06	0.45	2.08	0.33	2.04	0.24	2.06	0.16
5.08	0.85	5.12	0.59	4.98	0.42	5.09	0.28
1.00	0.29	1.02	0.21	0.99	0.17	1.04	0.12
						0.24	0.06

Table 7. Experimental data of hydrogen adsorption equilibrium on UiO-66(Zr)_$(COOH)_2$ at 269, 303, 333, and 373 K

T = 269 K		T = 303 K		T = 333 K		T = 373 K	
P	q	P	q	P	q	P	q
(bar)	(mmol·g^{-1})	(bar)	(mmol·g^{-1})	(bar)	(mmol·g^{-1})	(bar)	(mmol·g^{-1})
0.01	0.00	0.02	0.00	0.02	0.00	0.01	0.00
1.63	0.07	1.45	0.03	1.26	0.02	0.56	0.00
5.15	0.10	5.17	0.07	5.80	0.04	1.05	0.00
20.32	0.15	5.15	0.07	20.16	0.08	5.36	0.01
30.35	0.17	20.36	0.11	30.54	0.10	20.05	0.04
15.07	0.13	30.77	0.13	14.67	0.07	30.85	0.07
7.51	0.11	14.86	0.09	7.38	0.06	30.86	0.07
		7.04	0.08			15.02	0.03
						7.43	0.02

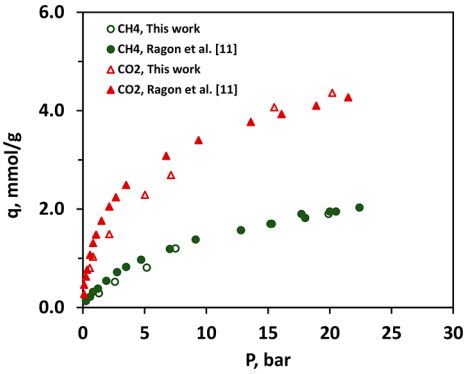

Figure 6. Comparison of the adsorption equilibrium isotherms on UiO-66(Zr)_$(COOH)_2$ at 303 K for carbon dioxide and methane with data reported in this work and data reported by Ragon et al.[11]

explanation for the fact that the DSS model is the most suitable model used to fit the experimental data.

$$q_i = q_{\text{sat},1}\frac{(b_1P)^{1/n_1}}{1 + (b_1P)^{1/n_1}} + q_{\text{sat},2}\frac{(b_2P)^{1/n_2}}{1 + (b_2P)^{1/n_2}} \quad (5)$$

In this equation, q_i is the adsorbed phase concentration in the micropores and P is the partial pressure. b_1 and b_2 are the adsorption equilibrium constants for the two site types. Similarly, $q_{\text{sat},1}$ and $q_{\text{sat},2}$ are the saturation capacities of each site, and coefficients n_1 and n_2 represent the solid heterogeneity parameters. Because the experimental adsorption equilibrium results were obtained over a large temperature range, the temperature dependence of the equilibrium parameters is also required. Each parameter b can be obtained from eq 6.[22]

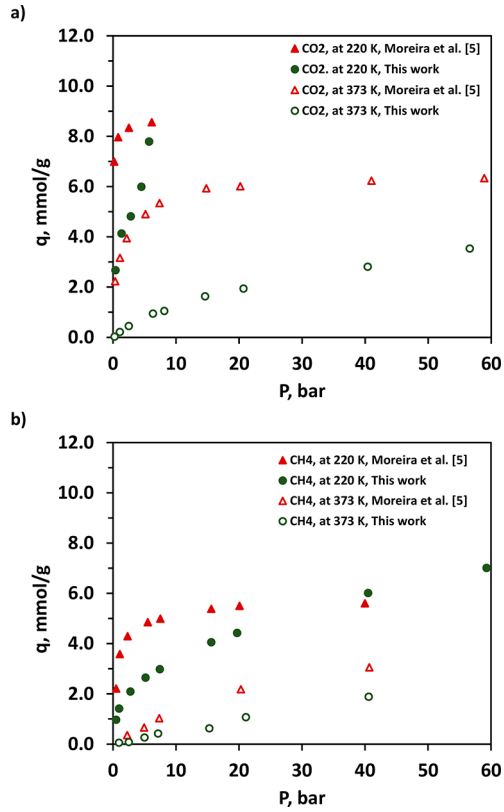

Figure 7. Comparison of the adsorption equilibrium isotherms on UiO-66(Zr)_$(COOH)_2$ at 220 and 373 K for (a) carbon dioxide and (b) methane, with data reported in this work and data reported by Moreira et al.[5] for binderless zeolite 13X.

DOI: 10.1021/acs.jced.9b00053
J. Chem. Eng. Data 2019, 64, 4724−4732

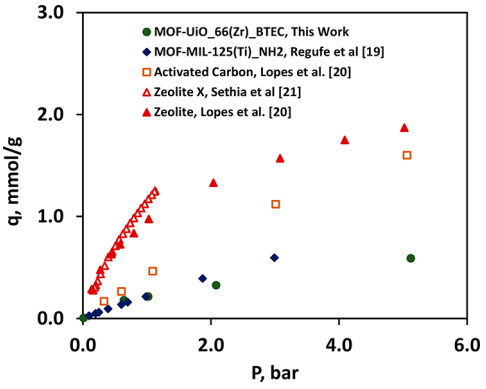

Figure 8. Comparison of the adsorption equilibrium isotherms on UiO-66(Zr)_$(COOH)_2$ at 303 K for carbon monoxide with data reported in this work and data reported by Lopes et al. on activated cardon and on a zeolite[20] by Regufe et al. on MOF MIL-125(Ti)-NH_2[19] and by Sethia et al. on zeolite X.[21]

$$b = b_0 \exp\left(\frac{-\Delta H}{R_g \times T}\right) \quad (6)$$

b_0 is the affinity at infinite temperature, R_g is the ideal gas constant, and $-\Delta H$ is the parameter related to the heat of adsorption. The temperature dependency of the heterogeneity parameter (n) can be described by the empirical correlation shown in eq 7, where T_0 is the reference temperature (T_0 = 303 K).[22]

$$\frac{1}{n} = \frac{1}{n_0} + \alpha\left(1 - \frac{T_0}{T}\right) \quad (7)$$

To determine DSS model parameters, it was necessary to perform the regression of the model against the experimental data for each component. The adjusting parameters can be found in Table 8. As can be seen, the experimental data was well described by the DSS model shown as lines in Figure 5.

The isosteric heat of adsorption represents the interaction strength between the adsorbate molecules and the adsorbent surface, giving valuable information about the energetic heterogeneity of the adsorbent surface. This parameter can be calculated from the Clausius−Clapeyron equation (eq 8).[22]

$$\frac{-\Delta H}{R_g T^2} = \left(\frac{\partial \ln P}{\partial T}\right)_q \quad (8)$$

The isosteric heat of adsorption for each component was determined from the experimental adsorption data of CH_4, CO_2, N_2, and CO over UiO-66(Zr)_$(COOH)_2$ as a function of the loading (Figure 9).

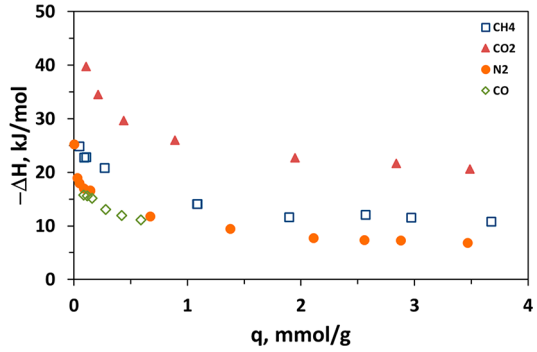

Figure 9. Isosteric heats of adsorption for carbon dioxide, methane, nitrogen, and carbon monoxide on UiO-66(Zr)_$(COOH)_2$.

Ragon et at.[11] reported adsorption enthalpies for CO_2 and CH_4 at 303 K as a function of loading, assessed by microcalorimetry. The experiments reported by Ragon and co-workers were performed in powder sample, also outgassed at 423 K. They reported that the heat of adsorption decreases with loadings of between 35 and 30 kJ·mol^{-1} for CO_2 (corresponding to loadings of 0.2 and 4 mmol·g^{-1}, respectively), while for CH_4 they report a more constant pattern (i.e, heat of adsorption of about 23.3 kJ·mol^{-1} for a loading of 0.1 mmol·g^{-1}, and 20.3 kJ·mol^{-1} for a loading of 1 mmol·g^{-1}). These values are in good agreement with the isosteric heats of adsorption reported on this work for CO_2, but for CH_4 this good agreement is verified only for low loadings. Regarding H_2, a value of the isosteric heat of adsorption of 20 kJ/mol was obtained. This value is high when compared to values reported for other MOFs, which range from 6 to 13 kJ/mol.

CONCLUSIONS

Single adsorption equilibrium isotherms of carbon dioxide, methane, carbon monoxide, nitrogen, and hydrogen on UiO 66(Zr)_$(COOH)_2$ agglomerates were measured by the gravimetric method in the temperature range of 223 to 273 K at up to 60 bar. The adsorption equilibrium model that best represented the experimental data is the dual-site Sips (DSS) model. It is noted that the adsorbent presents a higher adsorption capacity for carbon dioxide, followed by methane, nitrogen, carbon monoxide, and hydrogen. The isosteric heat of adsorption for each component was determined, and as expected, a higher value for carbon dioxide was obtained.

Table 8. Parameters of the Dual-Site Sips Isotherm for UiO-66(Zr)_$(COOH)_2$

parameter	CO_2	CH_4	N_2	CO	H_2	units
$q_{0,1}$	4.96	10.46	0.90	1.84	0.21	mmol·g^{-1}
$q_{0,2}$	5.34	6.89	7.65	0.52	0.42	mmol·g^{-1}
$b_{0,1}$	1.50×10^{-5}	1.42×10^{-4}	5.36×10^{-4}	3.81×10^{-3}	3.12×10^{-5}	bar^{-1}
$b_{0,2}$	5.62×10^{-5}	5.89×10^{-5}	1.49×10^{-3}	9.41×10^{-4}	2.41×10^{-5}	bar^{-1}
$-\Delta H_1$	23.5	7.0	7.0	7.3	18.9	kJ·mol^{-1}
$-\Delta H_2$	15.0	11.8	4.7	15.7	13.9	kJ·mol^{-1}
$n_{0,1}$	1.35	1.00	0.24	0.49	1.45	
$n_{0,2}$	0.45	1.57	1.01	1.52	0.35	
α_1	0.67	0.00	0.00	1.04	1.54	
α_2	0.00	0.50	0.90	0.00	0.11	

DOI: 10.1021/acs.jced.9b00053
J. Chem. Eng. Data 2019, 64, 4724−4732

■ ASSOCIATED CONTENT

Supporting Information

The Supporting Information is available free of charge on the ACS Publications website at DOI: 10.1021/acs.jced.9b00053.

Details on the UiO-66(Zr)_$(COH)_2$ powder characterization and a brief summary of hydrogen adsorption on MOFs at ambient temperature (PDF)

■ AUTHOR INFORMATION

Corresponding Authors

*E-mail: jschang@krict.re.kr.

*E-mail: arodrig@fe.up.pt.

ORCID

U.-Hwang Lee: 0000-0002-2779-8142

A. M. Ribeiro: 0000-0003-4269-1420

A. F. P. Ferreira: 0000-0002-6746-8973

A. E. Rodrigues: 0000-0002-0715-4761

Funding

This work is a result of Project "AIProcMat@N2020 - Advanced Industrial Processes and Materials for a Sustainable Northern Region of Portugal 2020", with the reference NORTE-01-0145-FEDER-000006, supported by Norte Portugal Regional Operational Programme (NORTE 2020), under the Portugal 2020 Partnership Agreement, through the European Regional Development Fund (ERDF); Project NORTE-01-0145-FEDER-029384 funded by FEDER funds through NORTE 2020 - Programa Operacional Regional do NORTE and by national funds (PIDDAC) through FCT/MCTES; and Associate Laboratory LSRE-LCM - UID/EQU/50020/2019, funded by national funds through FCT/MCTES (PIDDAC). J.-S.C. is grateful to the Center for Convergent Chemical Process (CCP, grant no. SKC1810-4) for financial support.

Notes

The authors declare no competing financial interest.

■ REFERENCES

(1) Bobbitt, N. S.; Chen, J.; Snurr, R. Q. High-Throughput Screening of Metal−Organic Frameworks for Hydrogen Storage at Cryogenic Temperature. *J. Phys. Chem. C* **2016**, *120* (48), 27328−27341.

(2) Li, H.; et al. Recent advances in gas storage and separation using metal−organic frameworks. *Mater. Today* **2018**, *21* (2), 108−121.

(3) Suh, M. P.; et al. Hydrogen Storage in Metal−Organic Frameworks. *Chem. Rev.* **2012**, *112* (2), 782−835.

(4) Grande, C. A.; Blom, R. Cryogenic Adsorption of Methane and Carbon Dioxide on Zeolites 4A and 13X. *Energy Fuels* **2014**, *28* (10), 6688−6693.

(5) Moreira, M. A.; et al. Cryogenic pressure temperature swing adsorption process for natural gas upgrade. *Sep. Purif. Technol.* **2017**, *173*, 339−356.

(6) *DOE Technical Targets for Onboard Hydrogen Storage for Light-Duty Vehicles*. [cited October 22, 2018]; Available from https://www.energy.gov/eere/fuelcells/doe-technical-targets-onboard-hydrogen-storage-light-duty-vehicles.

(7) Mason, J. A.; Veenstra, M.; Long, J. R. Evaluating metal−organic frameworks for natural gas storage. *Chemical Science* **2014**, *5* (1), 32−51.

(8) Pirngruber, G. D.; Llewellyn, P. L. Opportunities for MOFs in CO_2 Capture from Flue Gases, Natural Gas, and Syngas by Adsorption. In *Metal-Organic Frameworks: Applications from Catalysis to Gas Storage*; Farrusseng, D., Ed.; Wiley-VCH: Weinheim, Germany, 2011; p 99.

(9) Yang, Q.; et al. A Water Stable Metal−Organic Framework with Optimal Features for CO2 Capture. *Angew. Chem., Int. Ed.* **2013**, *52* (39), 10316−10320.

(10) Hu, Z.; et al. A Modulated Hydrothermal (MHT) Approach for the Facile Synthesis of UiO-66-Type MOFs. *Inorg. Chem.* **2015**, *54* (10), 4862−4868.

(11) Ragon, F.; et al. Acid-functionalized UiO-66(Zr) MOFs and their evolution after intra-framework cross-linking: structural features and sorption properties. *J. Mater. Chem. A* **2015**, *3* (7), 3294−3309.

(12) Wiersum, A. D.; et al. An Evaluation of UiO-66 for Gas-Based Applications. *Chem. - Asian J.* **2011**, *6* (12), 3270−3280.

(13) Cavka, J. H.; et al. A New Zirconium Inorganic Building Brick Forming Metal Organic Frameworks with Exceptional Stability. *J. Am. Chem. Soc.* **2008**, *130* (42), 13850−13851.

(14) Kandiah, M.; et al. Synthesis and Stability of Tagged UiO-66 Zr-MOFs. *Chem. Mater.* **2010**, *22* (24), 6632−6640.

(15) Wiersum, A. *Developing a Strategy to Evaluate the Potential of New Porous Materials for the Separation of Gases by Adsorption*. Ph.D. Thesis, Sciences des Matériaux, Physique, Chimie et Nanosciences, 2012.

(16) Dubinin, M. M.; et al. Study of the adsorptional properties and secondary porous structure of adsorbents with a molecular sieve action. *Bull. Acad. Sci. USSR, Div. Chem. Sci.* **1961**, *10* (8), 1293−1299.

(17) Al-Baghli, N. A.; Loughlin, K. F. Adsorption of Methane, Ethane, and Ethylene on Titanosilicate ETS-10 Zeolite. *J. Chem. Eng. Data* **2005**, *50* (3), 843−848.

(18) Ferreira, A. F. P.; et al. Suitability of Cu-BTC extrudates for propane−propylene separation by adsorption processes. *Chem. Eng. J.* **2011**, *167* (1), 1−12.

(19) Regufe, M. J.; et al. Syngas Purification by Porous Amino-Functionalized Titanium Terephthalate MIL-125. *Energy Fuels* **2015**, *29* (7), 4654−4664.

(20) Lopes, F. V. S.; et al. Adsorption of H2, CO2, CH4, CO, N2 and H2O in Activated Carbon and Zeolite for Hydrogen Production. *Sep. Sci. Technol.* **2009**, *44* (5), 1045−1073.

(21) Sethia, G.; Somani, R. S.; Bajaj, H. C. Adsorption of carbon monoxide, methane and nitrogen on alkaline earth metal ion exchanged zeolite-X: structure, cation position and adsorption relationship. *RSC Adv.* **2015**, *5* (17), 12773−12781.

(22) Do, D. D. In *Adsorption Analysis: Equilibria and Kinetics*; Yang, R. T., Ed.; Series on Chemical Engineering; Imperial College Press: London, 1998.

DOI: 10.1021/acs.jced.9b00053
J. Chem. Eng. Data 2019, 64, 4724−4732